JOURNAL OF SOLID STATE CHEMISTRY **129,** 105–112 (1997)
ARTICLE NO. SC967237

High Oxygen Pressure Preparation, Structural Refinement, and Thermal Behavior of $R\mathrm{Mn_2O_5}$ (R = La, Pr, Nd, Sm, Eu)

J. A. Alonso,[1] M. T. Casais, M. J. Martínez-Lope, and I. Rasines

Instituto de Ciencia de Materiales de Madrid, C.S.I.C., Cantoblanco, E-28049 Madrid, Spain

Received July 1, 1996; in revised form November 18, 1996; accepted November 19, 1996

The title compounds have been prepared in powder form by a citrate technique followed by a high oxygen pressure (P = 200 bar) treatment. The La and Pr compounds are described for the first time. X-ray powder diffraction data are given, as well as the results of the Rietveld analysis of the patterns. All the phases are isostructural (space group *Pbam*), containing in the crystal structure infinite chains of $Mn^{4+}O_6$ octahedra sharing edges, linked together by $Mn^{3+}O_5$ and RO_8 units. All the studied compounds are electrical insulators. The thermal analysis of the samples enabled us to determine the oxidation state of Mn, which is slightly higher than expected, suggesting the presence of some oxygen excess in the structure.

INTRODUCTION

In the course of our current research on $R\mathrm{MnO_3}$ (R = La, Pr, Nd) perovskites we identified, after synthesis processes at high oxygen pressures, minor impurity phases isostructural with $\mathrm{YMn_2O_5}$ (1). The lack of X-ray powder diffraction data (XRD) for $R\mathrm{Mn_2O_5}$ (R = rare earths) and the incomplete characterization of most of these interesting phases led us to undertake a systematic study on its structural, electrical, and magnetic properties.

The $R\mathrm{Mn_2O_5}$ family of oxides was first described by Quezel-Ambrunaz *et al.* (2) and Bertaut *et al.* (3), who prepared single-crystal phases from a $\mathrm{Bi_2O_3}$ flux for R = rare earths, and gave the unit-cell parameters for the complete series. The authors already recognized the extraordinary flexibility of the structure concerning the substitutions of both R and Mn atoms allowing, for instance, the preparation of $R\mathrm{MnTiO_5}$ phases.

The crystal structure of the isomorphic series was solved for $\mathrm{HoMn_2O_5}$ (2) and subsequently refined for other rare earths: $\mathrm{DyMn_2O_5}$ (4), $\mathrm{ErMn_2O_5}$, and $\mathrm{TbMn_2O_5}$ (5) and, more recently, $\mathrm{NdMn_2O_5}$ (6). All these studies were performed from single-crystal data. The structure is orthorhombic and contains two kinds of crystallographic positions for Mn. Mn1 is hexacoordinated to oxygens forming $\mathrm{Mn1O_6}$ distorted octahedra. The coordination of Mn2 is best described as slightly distorted tetragonal pyramidal. From considerations relating the Mn–O distances and the observed magnetic couplings, it can be assumed that Mn1 positions correspond to tetravalent Mn cations, whereas Mn2 are occupied by Mn^{3+} cations. In the global crystal structure [$Mn^{4+}O_6$] octahedra form infinite chains parallel to the c axis, linked through [$Mn^{3+}O_5$] units and bicapped [RO_8] antiprisms. The shortest metal–metal distance noticed in this family is Mn1–Mn1 = 2.750(2) Å in the Nd compound. Important implications on the physical properties of these phases can be presumed from such short distances. The magnetic structures, studied for R = Nd (7), Dy (8), Tb, and Er (5,7) from neutron diffraction data, are rather complex and show amplitude modulation of the ordered magnetic moments.

The aim of this paper is to describe the preparation of polycristalline samples of $R\mathrm{Mn_2O_5}$ for La and the lighter rare earths (R = Pr, Nd, Sm, Eu), which can be only (for R = La) or better (R = Pr...Eu) prepared under high oxygen pressure. XRD data are given, as well as the result of the Rietveld refinements of the crystal structures. The thermal and electrical behaviors are also reported.

EXPERIMENTAL

$R\mathrm{Mn_2O_5}$ (R = La, Pr, Nd, Sm, Eu) phases were obtained as dark brown polycrystalline powders starting from precursors previously synthesized by a citrate technique. Stoichiometric amounts of analytical grade R_2O_3 and $\mathrm{Mn(NO_3)_2 \cdot 4H_2O}$ were solved in citric acid. The citrate solutions were slowly evaporated and decomposed at temperatures up to 600°C. All the organic materials were eliminated in a subsequent treatment at 800°C in air. High oxygen pressure treatments were performed in a Morris Research furnace, HPS-3210. About 2 grams of the precursor powders were contained in a gold can during the oxygenation processes. The samples were slowly heated up to

[1] To whom correspondence should be addressed.

0022-4596/97 $25.00

1000° at a final oxygen pressure of 200 bar, and held at this temperature for 12 h. The products were finally cooled, under pressure, at 300°C h^{-1} down to room temperature. Finally, the oxygen pressure was slowly released. Parallel treatments were also performed in air at temperatures up to 1000°C.

X-ray powder diffraction (XRD) patterns were collected with Cu$K\alpha$ radiation in a Siemens D-501 goniometer controlled by a DACO-MP computer. For the structural refinements the diagrams were recorded by step-scanning from 10 to 100° in 2θ, in increments of 0.05° and a counting time of 4 s each step. The XRD patterns were analyzed by the Rietveld (9) method, using the FULLPROF program (10), a strongly modified version of the Young and Wiles code (11). A pseudo-Voigt function was chosen to generate the line shape of the diffraction peaks. No regions were excluded in the refinements. In the final run the following parameters were refined: background coefficients, zero-point, half-width, pseudo-Voigt, and asymmetry parameters for the peak shape; scale factor, positional, and unit-cell parameters. Isotropic thermal factors were set to 0.3 and 0.7 $Å^2$ for metals and oxygens atoms, respectively, and an overall thermal factor was also refined.

Thermal analysis was carried out in a Mettler TA3000 system equipped with a TC10 processor unit. Thermogravimetric (TG) curves were obtained in a TG50 unit, working at a heating rate of 10°C min^{-1}, in a reducing $H_2(5\%)/N_2(95\%)$ flow of 0.3 l min^{-1}. About 30 mg of sample were used in each experiment.

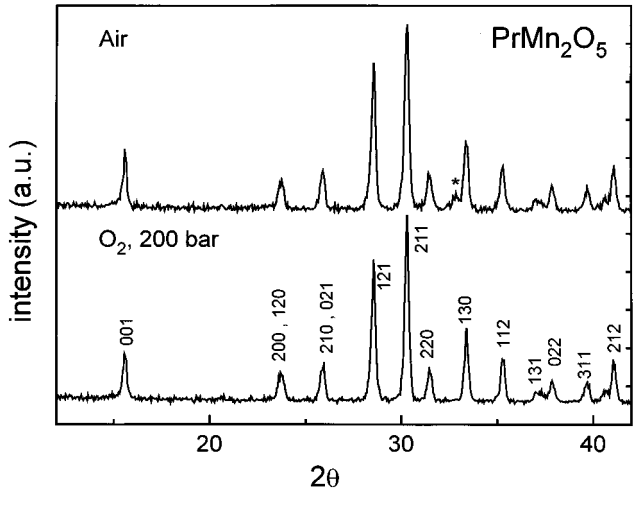

FIG 1. XRD patterns of $PrMn_2O_5$ prepared by heating citrate precursors either in air or under 200 bar O_2 at 1000°C. The star indicates the most intense reflection of the competitive $PrMnO_3$ perovskite, identified as a minor phase only after the treatment in air. The pattern of the pure $PrMn_2O_5$ phase is indexed in an orthorhombic unit cell with **a** = 7.5583(9), **b** = 8.6481(9), **c** = 5.7119(6) Å.

RESULTS AND DISCUSSION

Preparation

The preparation of pure RMn_2O_5 phases has shown to be extremely favored by (i) the use of finely divided and homogeneous precursors and (ii) the final thermal treatment under high oxygen pressure. The last condition is specially essential in the preparation of $LaMn_2O_5$, which could not be obtained at ambient pressure starting either from citrate precursors or ceramic mixtures: the competitive $LaMnO_3$ perovskite and MnO were always identified after all the thermal treatments in air at different temperatures. The remaining RMn_2O_5 oxides (R = Pr, Nd, Sm, Eu) could be prepared as major phases, together with $RMnO_3$ as impurities, by heating in air the citrate precursors (up to 1000°C), but single-phased products could be achieved only by subsequent annealing of the samples at 1000°C under 200 bar of O_2. Figure 1 shows the XRD pattern for a $PrMn_2O_5$ sample prepared either in air, where the competitive $PrMnO_3$ phase is still present, or in high oxygen pressure (200 bar), where a single-phased product is obtained. This behavior can be understood since the application of oxygen pressure favors the stabilization of the high oxidation states of manganese, Mn^{3+} and Mn^{4+}.

Figure 2 shows the XRD patterns of RMn_2O_5 (R = La, Pr, Nd, Sm, Eu). They all correspond to pure phases that

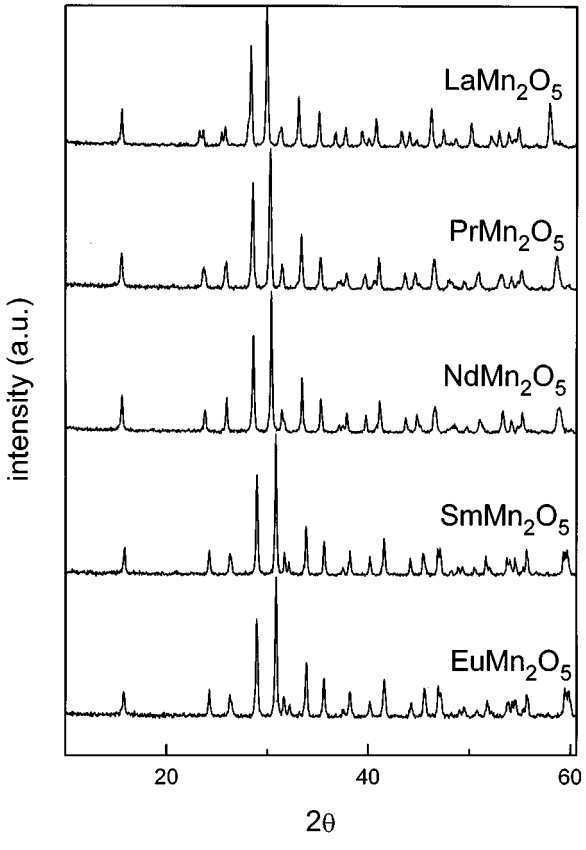

FIG. 2. X-ray powder diffraction data for RMn_2O_5.

can be indexed in an orthorhombic unit-cell isotypic to YMn_2O_5 (1), with no additional peaks which could indicate the presence of superstructures or departure of the mentioned symmetry. The observed d-spacings and intensities for the reflections in the 2θ range between 10 and 60° are listed in Table 1.

Crystal Structure Refinement

The crystal structure of the five compounds was refined by profile analysis taking as starting structural model that of $NdMn_2O_5$ (6), in the space group *Pbam* (No. 55), $Z = 4$. An example of the good agreement between the observed and calculated profiles of the pattern is given in Fig. 3 for $LaMn_2O_5$ and $PrMn_2O_5$.

The refined unit-cell parameters are listed in Table 2, and plotted in Fig. 4 versus the ionic radii of the rare-earth cations (12). There is an almost linear variation of **a**, **b**, **c**, and **V**, according to the well-known lanthanide contraction. It is noteworthy that the observed cell parameters in our powder patterns are significantly different from those reported in the literature, from single crystal samples, included also in the same Table 2. It is possible that the way of preparation of these crystals (3, 6), involving a Bi_2O_3 flux (3) or manganese halides (6) could have led to small substitutional incorporation of strange atoms into the structure, thus modifying slightly the size of the cell.

The final atomic coordinates after the refinement are listed in Table 3. Final bonding distances and angles are given in Table 4. A representation of the structure is shown in Fig. 5. $Mn1O_6$ octahedra share edges via O2 and O3 oxygens, to form infinite chains running along the c axis. The chains are linked together by $Mn2O_5$ units, through O3 and O4 oxygens. In fact, $Mn2O_5$ pyramids share edges through common O1 oxygens to form dymer units, $Mn2_2O_8$, as shown in Fig. 5. The bigger R atoms are at the eightfold coordinated holes of the network.

TABLE 1
X-Ray Powder Diffraction Data for RMn_2O_5

R	La		Pr		Nd		Sm		Eu	
hkl	d_{obs}	I/I_0	d_{obs}	I/I_0	d_{obs}	I/I_0	d_{obs}	I/I_0	d_{obs}	I/I_0
001	5.73	31	5,72	29	5.71	27	5.69	20	5.69	19
200	3.85	15								
120	3.78	14	3.76	18	3.74	17	3.72	19	3.70	21
210	3.51	12								
021	3.46	16	3.45	22	3.44	25	3.43	15	3.40	14
121	3.16	82	3.13	79	3.13	62	3.12	72	3.10	65
211	2.998	100	2.956	100	2.944	100	2.932	100	2.909	100
002	2.865	17	2.848	19	2.846	16	2.849	15	2.842	16
220							2.813	11	2.791	11
130	2.717	42	2.688	47	2.680	32	2.676	35	2.657	40
112	2.560	30	2.552	28	2.545	24	2.541	25	2.529	29
131	2.458	11	2.436	8	2.423	7	2.420	7	2.404	7
022	2.390	17	2.383	15	2.377	15	2.374	15	2.364	19
202	2.292	14	2.277	13	2.272	10	2.264	12	2.255	13
311	2.260	7	2.224	9						
212	2.220	24	2.198	24	2.197	23	2.190	27	2.181	28
140	2.097	14	2.077	15	2.072	12	2.063	11	2.055	12
321	2.059	13	2.033	15	2.025	14	2.009	14	1.994	21
222	2.030	6	2.011	6						
132							1.951	20	1.944	21
141	1.967	32	1.954	27	1.949	19	1.941	20	1.934	18
330	1.921	13	1.901	7	1.895	4	1.875	7	1.865	6
400			1.892	8	1.886	6	1.859	7	1.847	8
410	1.878	8	1.844	9	1.832	5	1.819	7	1.805	7
331	1.822	19	1.794	15	1.790	10	1.780	15	1.773	13
420	1.759	11					1.715	14	1.710	12
042	1.733	13	1.726	14	1.720	17	1.708	12	1.698	11
123	1.706	14	1.696	12	1.695	10	1.694	13	1.685	14
213	1.675	18	1.668	18	1.665	15	1.661	18	1.656	18
332	1.594	37	1.576	30	1.569	19	1.566	18	1.560	20
402							1.558	18	1.550	19

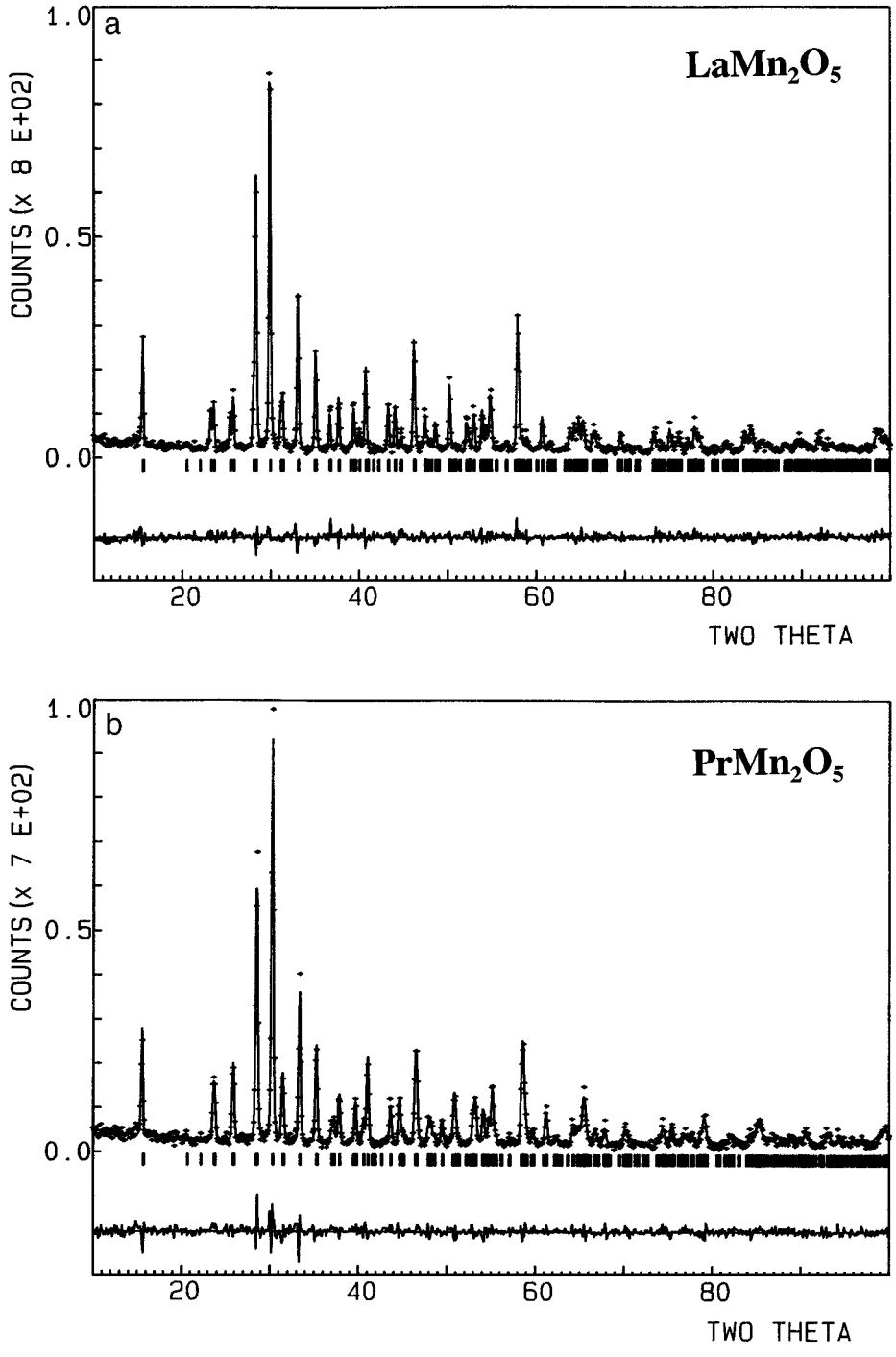

FIG. 3. Observed (crosses), calculated (solid line), and difference (at the bottom) XRD profiles for (a) $LaMn_2O_5$ and (b) $PrMn_2O_5$ at 295 K. The tick marks indicate the positions of the allowed Bragg reflections. For the sake of clarity only half of the experimental points are represented.

The relatively high standard deviations of the oxygen positions, associated to the small scattering factor of oxygen in front of *R* and Mn atoms, and the limitations inherent to powder diffraction, make it difficult to observe definite trends in the individual metal-to-oxygen bond distances (Table 4) along the compounds of the series. However, some general remarks can be drawn. In the $Mn1O_6$ octahedra, the two Mn1–O3 bonds are significantly shorter than the four remaining Mn–O bonds. Similarly flattened octahedra have also been observed in other Mn^{4+}-containing structures,

TABLE 2
Unit-Cell Parameters and Volume for RMn_2O_5

R	**a** (Å)	**b** (Å)	**c** (Å)	**V** (Å)^3
La	7.6891(7)	8.7142(7)	5.7274(5)	383.76(9)
	7.67[a]	8.66	5.72	381.26
Pr	7.5583(9)	8.6481(9)	5.7119(6)	373.4(1)
	7.54[a]	8.66	5.70	372.19
Nd	7.5116(8)	8.6270(8)	5.7060(5)	369.76(9)
	7.54[a]	8.63	5.70	370.90
	7.471(1)[b]	8.588(2)	5.684(1)	364.7(1)
Sm	7.4332(7)	8.5872(7)	5.6956(5)	363.55(9)
	7.41[a]	8.56	5.70	361.55
Eu	7.3986(8)	8.5666(9)	5.6925(6)	360.8(1)
	7.37[a]	8.56	5.70	359.60

[a] From Ref. 3.
[b] From Ref. 6.

such as β-MnO_2 (rutile-type (13)), in which the octahedra form infinite chains by edge sharing too. $Mn2O_5$ pyramids also show very significantly different bond lengths: four oxygen atoms (2O1 + 2O4) are in a square plane, with Mn–O distances between 1.83 and 1.93 Å, and the fifth oxygen atom is in axial position at a longer distance from Mn, between 2.04 and 2.14 Å. In addition, looking at the

TABLE 3
Structural Parameters after the Rietveld Refinement of XRD Data for RMn_2O_5 Oxides

Atom		La	Pr	Nd	Sm	Eu
R	x	0.1468(5)	0.1442(6)	0.1420(6)	0.1413(6)	0.1401(7)
	y	0.1729(6)	0.1729(6)	0.1738(7)	0.1720(7)	0.1715(7)
Mn1	z	0.2636(18)	0.2601(20)	0.2603(19)	0.2640(21)	0.2625(22)
Mn2	x	0.4107(10)	0.4147(11)	0.4092(12)	0.4109(13)	0.4120(13)
	y	0.3511(12)	0.3493(13)	0.3544(12)	0.3505(14)	0.3474(15)
O1	z	0.2848(64)	0.2894(69)	0.2879(69)	0.2988(70)	0.3074(72)
O2	x	0.1476(52)	0.1497(62)	0.1602(62)	0.1654(63)	0.1702(63)
	y	0.4488(44)	0.4479(47)	0.4538(52)	0.4460(50)	0.4458(52)
O3	x	0.1496(54)	0.1523(63)	0.1529(65)	0.1468(75)	0.1418(80)
	y	0.4366(37)	0.4416(42)	0.4319(43)	0.4307(46)	0.4374(47)
O4	x	0.4072(29)	0.4080(34)	0.4012(33)	0.4042(38)	0.3957(40)
	y	0.2039(30)	0.2081(31)	0.2003(34)	0.2041(36)	0.2048(38)
	z	0.2580(37)	0.2551(39)	0.2532(38)	0.2583(41)	0.2616(41)
χ^2		1.28	1.22	1.28	1.30	1.29
R_I(%)[a]		6.49	6.73	6.61	8.23	8.71

Note. R and O2 atoms are at 4g ($x, y, 0$) positions; Mn1 at 4f ($0, 1/2, z$); Mn2 and O3 at 4h ($x, y, 1/2$); O1 at 4e ($0, 0, z$) and O4 at 8i (x, y, z) positions.
[a] Bragg R_I factor is given over 420 reflections.

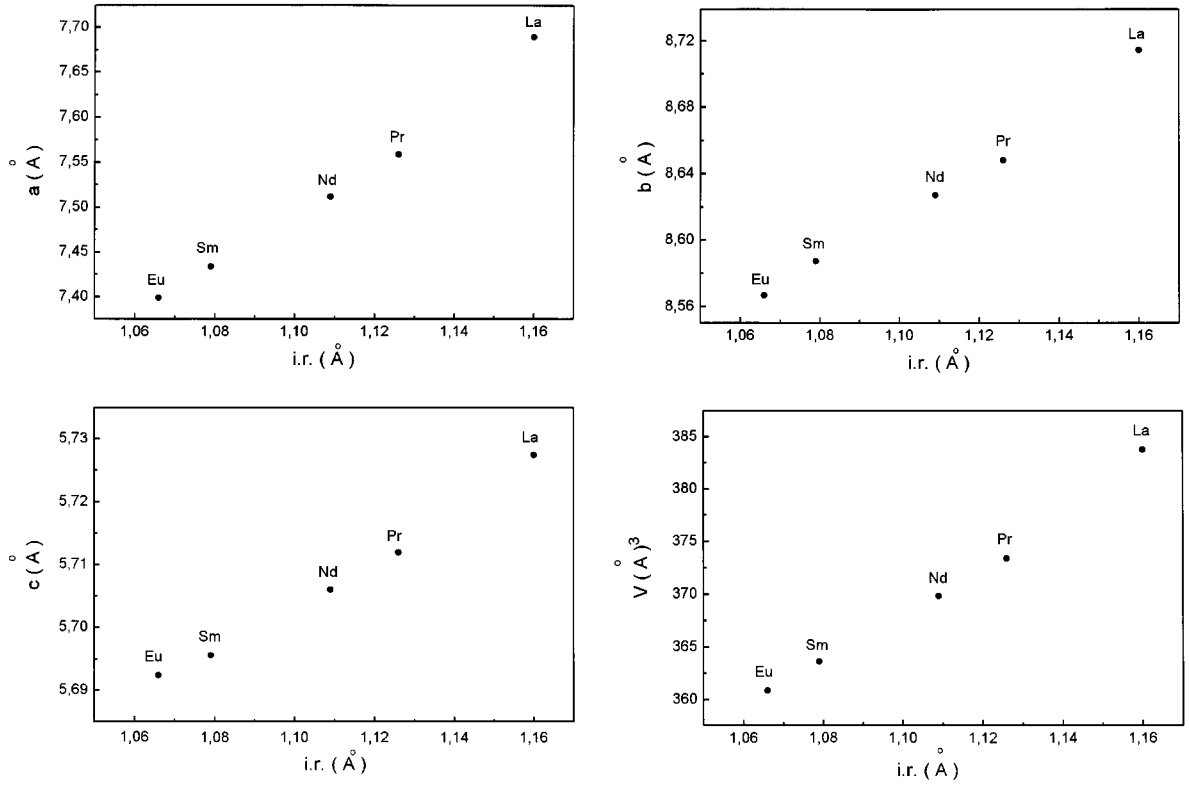

FIG 4. Unit-cell parameters and volume variation with the ionic radii of R.

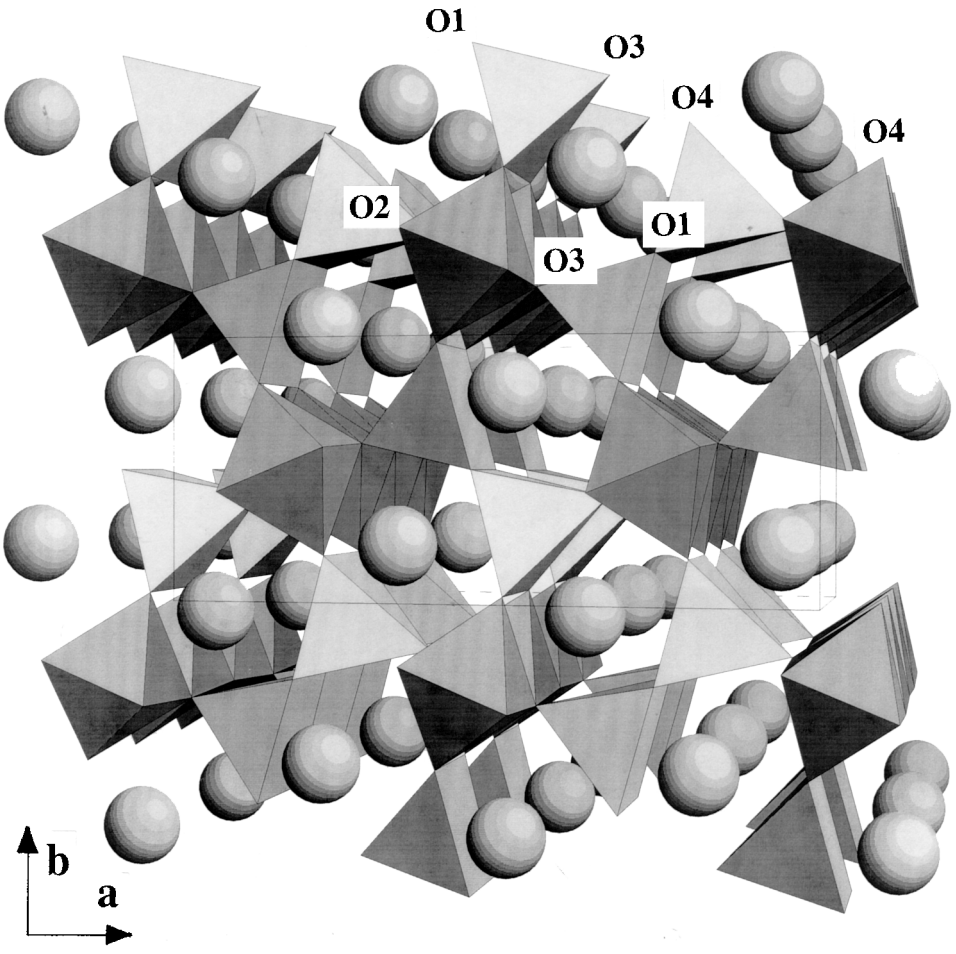

FIG. 5. Projection of the RMn_2O_5 structure, approximately along the *c* axis. Octahedra and tetragonal pyramids correspond to $Mn1O_6$ and $Mn2O_5$ units, respectively.

average metal–oxygen distances within each coordination polyhedron, we observe that both RO_8 and $Mn2O_5$ polyhedra have a tendency to decrease in size from La to Eu. This is related to the lanthanide contraction which correspondingly scales with the size of the unit cell.

The observed Mn1–Mn1 distances are extremely short, in the range 2.70–2.75 Å. They are much smaller than the Mn–Mn contact in other comparable phases, such as 2.871 Å in β-MnO_2 (13). It is evident the influence that such structural features can have in the magnetic interactions between manganese cations. The magnetic susceptibility and the ordered magnetic structures will be studied in the inmediate future.

Transport measurements show that all the studied RMn_2O_5 (R = La...Eu) phases are insulating, with resistivities higher than 10^8 Ωcm. The variation of the electrical resistance with temperature was not measured.

Thermal Analysis

The thermal behavior of RMn_2O_5 in a reducing H_2/N_2 flow is illustrated in Fig. 6 for R = La. The TG curve shows two well-defined steps, starting at 275 and 650°C, respectively (Table 5). The DTG curve shows that, in fact, the first step is formed by two closely overlapping processes, with DTG peaks at 460 and 500°C. After the first step a plateau is observed, where a mixture of a bad-crystallized perovskite phase and MnO can be identified by XRD. After the second step, showing a DTG peak at 800°C, the reduction process is completed to give a mixture of La_2O_3 and MnO. A similar behavior is observed in the thermograms of the remaining RMn_2O_5 phases, although a considerable shift of the starting and DTG temperatures is observed depending of the nature of R, as shown in Table 5. For the Sm and Eu samples, the second step strongly overlaps with the first step

TABLE 4
Selected Interatomic Distances (Å) in RMn_2O_5

R		La	Pr	Nd	Sm	Eu
$Mn^{4+}O_6$ octahedra						
Mn1–O2	(×2)	1.939(27)	1.921(31)	1.961(32)	1.996(32)	2.007(33)
Mn1–O3	(×2)	1.861(28)	1.858(32)	1.877(33)	1.828(37)	1.796(38)
Mn1–O4	(×2)	1.913(26)	1.931(27)	1.884(27)	1.896(31)	1.921(32)
⟨Mn2–O⟩		1.904(27)	1.903(30)	1.907(31)	1.907(33)	1.908(34)
$Mn^{3+}O_5$ tetragonal pyramid						
Mn2–O1	(×2)	1.926(26)	1.893(28)	1.872(27)	1.848(27)	1.833(28)
Mn2–O3		2.143(41)	2.143(47)	2.043(49)	2.090(55)	2.147(58)
Mn2–O4	(×2)	1.894(25)	1.858(25)	1.936(27)	1.866(28)	1.831(29)
⟨Mn2–O⟩		1.957(29)	1.929(30)	1.932(31)	1.904(33)	1.895(34)
$R^{3+}O_8$ biccapped prism						
R–O1	(×2)	2.477(25)	2.473(28)	2.466(27)	2.478(28)	2.497(29)
R–O2		2.417(39)	2.380(41)	2.420(45)	2.363(44)	2.366(45)
R–O2		2.498(40)	2.488(44)	2.403(46)	2.409(45)	2.380(46)
R–O4	(×2)	2.504(22)	2.490(25)	2.434(25)	2.464(26)	2.424(27)
R–O4	(×2)	2.596(23)	2.522(25)	2.558(26)	2.525(27)	2.568(28)
⟨R–O⟩		2.509(27)	2.480(30)	2.467(31)	2.463(31)	2.466(31)
Mn–Mn distances						
Mn1–Mn1		2.716(15)	2.746(16)	2.734(16)	2.699(17)	2.716(18)
Mn2–Mn2		2.923(14)	2.903(15)	2.859(15)	2.879(16)	2.906(17)

in such a way that only a global reduction process can be distinguished.

In all these compounds, the total weight losses observed after the reduction to MnO can be used to have an estimate of the oxygen contents and, hence, of the oxidation state of Mn in the departure samples. The total oxygen loss per formula unit is, in all the cases, slightly higher than expected, which suggests that the studied phases are better described by the formula $RMn_2O_{5+\delta}$, as indicated in Table 5. The excess oxygen, δ, is somewhat larger in the Sm and Eu compounds.

TABLE 5
Starting and DTG Temperatures (°) of the Two Processes Observed by Thermal Analysis of RMn_2O_5 under Reducing Conditions

	1st process		2nd process			
R	Starts	DTG	Starts	DTG	Total O loss	Formula
La	275	460, 500	650	800	1.56	$LaMn_2O_{5.06}$
Pr	275	450, 520	600	660	1.56	$PrMn_2O_{5.06}$
Nd	275	440, 525	580	660	1.57	$NdMn_2O_{5.07}$
Sm	270	440, 540	—	—	1.63	$SmMn_2O_{5.13}$
Eu	260	[a], 590	—	—	1.62	$EuMn_2O_{5.12}$

[a] Broad shoulder.

Note. The total weight loss after both processes is given in oxygen atoms per formula, with an estimated error of ± 0.01. The determined composition of the departure phases is also included.

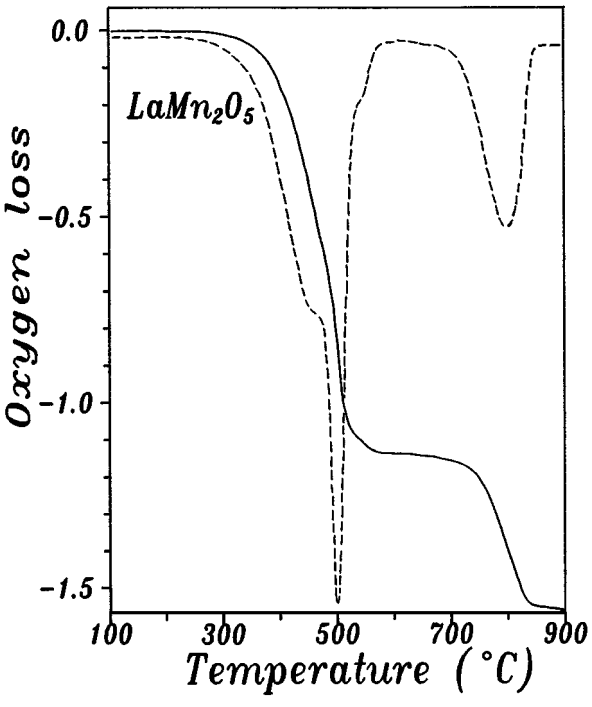

FIG. 6. TG (solid line) and DTG (broken line) curves obtained in a H_2/N_2 flow for $LaMn_2O_5$.

The global process observed during the total reduction of the samples can be written as

$$RMn_2O_{5+\delta} \xrightarrow{H_2} 1/2R_2O_3 + 2MnO + (1.5 + \delta)H_2O.$$

The excess oxygen of the departure samples may be incorporated in interstitial form into the structure. The determination of the structural location of such small amounts of interstitial oxygen atoms would require a detailed neutron diffraction study. The average oxidation state of Mn is in the range 3.56 + (for R = La) to 3.63 + (for R = Sm).

CONCLUSIONS

Polycrystalline RMn_2O_5 (R = La, Pr, Nd, Sm, Eu) samples have been prepared by thermal treatments under high oxygen pressure, necessary to better stabilize manganese in trivalent and tetravalent oxidation states. In the structure, Mn^{3+} and Mn^{4+} occupy different crystallographic positions, a square pyramidal environment and octahedral coordination, respectively. Thermal analysis in reducing conditions allowed us to determine the mean oxidation states for Mn, which are slightly higher than expected, ranging between 3.56 + and 3.63 + for the La and Sm compounds, respectively.

ACKNOWLEDGMENT

The authors acknowledge the financial support of the DGICYT to the Project PB94-0046.

REFERENCES

1. File Card No. 34-667 (YMn_2O_5), International Center for Diffraction Data, Newton Square, PA.
2. S. Quezel-Ambrunaz, E. F. Bertaut, and G. Buisson, *C. R. Acad. Sci.* **258,** 3025 (1964).
3. E. F. Bertaut, G. Buisson, A. Durif, A. Mareschal, M. C. Montmory, and S. Quezel-Ambrunaz, *Bull. Soc. Chim. Fr.* 1132 (1965).
4. S. C. Abrahams and J. L. Bernstein, *J. Chem. Phys.* **46,** 3776 (1967).
5. P. P. Gardner, C. Wilkinson, J. B. Forsyth, and B. M. Wanklyn, *J. Phys C* **21,** 5653 (1988).
6. P. Euzen, Ph. Leone, Ch. Gueho, and P. Palvadeau, *Acta Crystallogr. C* **49,** 1875 (1993).
7. G. Buisson, *Phys. Status Solidi A* **17,** 191 (1973).
8. C. Wilkinson, F. Sinclair, P. P. Gardner, J. B. Forsyth, and B. M. Wanklyn, *J. Phys. C* **14,** 1671 (1981).
9. H. M. Rietveld, *J. Appl. Crystallogr.* **2,** 65 (1969).
10. J. Rodríguez-Carvajal, *Physica B* **192,** 55 (1993).
11. D. B. Wiles and R. A. Young, *J. Appl. Crystallogr.* **14,** 149 (1981).
12. R. D. Shannon, *Acta Crystallogr. Sect. A* **32,** 751 (1976).
13. A. A. Bolzan, C. Fong, D. J. Kennedy, and C. J. Howard, *Aust. J. Chem.* **46,** 939 (1993).